Surface states in the optical spectra of two-dimensional photonic crystals with various surface terminations

S. A. Dyakov, A. Baldycheva, and T. S. Perova*
Department of Electronic and Electrical Engineering, Trinity College Dublin, Dublin 2, Ireland

G. V. Li and E. V. Astrova
Ioffe Physical Technical Institute, RAS, Polytekhnicheskaya 26, St. Petersburg, Russia

N. A. Gippius and S. G. Tikhodeev
A. M. Prokhorov General Physics Institute, RAS, Vavilova 38, Moscow, Russia

(Received 16 May 2012; revised manuscript received 22 August 2012; published 19 September 2012)

Reflection and transmission spectra of two-dimensional photonic crystal slabs, fabricated by photoelectrochemical etching of deep macropores and trenches in Si, are investigated theoretically and experimentally. It is shown that the presence of an unstructured silicon interfacial layer between the air and the photonic crystal structure can give rise to surface (Tamm) states within the TE and TM photonic stop bands. In the presence of roughness of inner surfaces of air pores, the surface states show up as dips within the stop bands in the reflection spectrum. The calculated electromagnetic near-field distribution demonstrates the vortices between the upper pores at the frequency of the surface mode. The experimental reflection and transmission spectra are in a good agreement with theoretical calculations performed by the Fourier modal method in the scattering matrix form.

DOI: 10.1103/PhysRevB.86.115126 PACS number(s): 42.70.Qs, 78.30.Fs, 11.55.−m, 82.45.−h

I. INTRODUCTION

The optical properties of photonic crystals depend on the geometry of their interfaces. This is a result of the breakdown of the translational symmetry of the spatial distribution of the dielectric permittivity, a primary characteristic of photonic crystals. The presence of the interface leads to appearance of the surface states. The Tamm surface states of photonic crystals were investigated theoretically in Refs. 1–7. These states were experimentally observed in Refs. 8–10. It was found that the Tamm surface states in a two-dimensional (2D) photonic crystal can affect the quality of point imaging by a photonic crystal slab (PCS) with negative refraction.[11,12] In Refs. 4 and 6, the enhancement of beaming via two-dimensional photonic crystal surface modes was studied. In Ref. 13 broad, surface-associated dips in the reflection spectra of colloidal photonic crystals were demonstrated. In Refs. 14 and 15, it was shown that surface modes generated in a thin layer of the photonic crystal material provide highly efficient coupling of light into a slow light mode of photonic crystal. This effect was used for the fabrication of a miniature gas sensor exhibiting an enhancement of CO_2 infrared absorption by a factor of 3. From these references, it is obvious, that the presence of surface states plays a crucial role in the optical characteristics of photonic crystals.

The goal of the present study is the experimental and theoretical investigation of the role of the surface (Tamm) states on the reflection and transmission spectra of the slabs of two-dimensional photonic crystals made of macroporous silicon. For this purpose, we manufactured slabs of macroporous silicon with a 2D array of cylindrical air pores and investigated their optical spectra both experimentally and theoretically. The reflection and transmission spectra of the samples were measured at a normal incidence of light, perpendicularly to the pore axis, with a Fourier transform infrared spectrometer coupled to an infrared microscope.

A theoretical model was constructed allowing for the structural properties such as the surfaces, limited thickness, and the inevitable roughness of the pores and surfaces. Accounting for roughness in the model is problematic and requires further discussion.

Rayleigh light scattering on rough surfaces can significantly decrease the reflection coefficient from a photonic crystal in the regions of the photonic stop bands. There are a number of publications[16–21] that show that these light losses are well accounted for by introduction of an imaginary part to the refractive indices of transparent materials. In the present paper a similar approach is used.

In order to model light propagation in a PCS, we employ the Fourier modal method in the scattering matrix form.[22,23] This method has proven to be very efficient for the investigation of semiconductor and metal/dielectric photonic crystal layers of finite thickness.[24,25]

The structure of the paper is as follows. In Sec. II, we describe our macroporous silicon structures, their manufacturing and the experimental setup. In Sec. III, we give a brief overview of the scattering matrix numerical method and the way how we describe the structure to simulate our experimental results. In Sec. IV, we present the numerical results for idealized structures, neglecting the roughness of the pores and surfaces. We show that reflection dips arise inside the stop bands in both polarizations, investigate their dependence on the width of the interfacial layer, and calculate the electromagnetic field distribution in the near-field zone. This analysis proves the surface Tamm character of the corresponding resonance states. In Sec. V we present the experimental results in comparison with the theoretical model. We show that the experimentally observed reflection spectra, especially in the vicinity of the surface mode dips, are very sensitive to the roughness losses and can be quantitatively reproduced by introduction of an imaginary part to the refractive index of silicon. In Sec. VI we

propose a simple model in order to explain why the surface state reflection dip are very sensitive to the roughness-caused losses.

II. EXPERIMENTAL METHODS

In order to fabricate 2D PCSs, we used joint photoelectrochemical etching of deep macropores and trenches in a silicon wafer.[26–29] As a starting material, we used n-Si (100) wafers of resistivity $\rho = 5\ \Omega\,\mathrm{cm}$ and a thickness of 250 μm. Nucleation centers were formed by photolithography followed by anisotropic etching in a hot aqueous alkaline solution. The mask layer was silicon dioxide formed by plasma-enhanced chemical vapor deposition. The triangular lattice of nucleation centers for macropores (pits) had a period of $a = 3.75\ \mu$m. The choice of another geometrical parameter, namely the distance between the nucleation grooves for trenches and the centers of the nearest row of pits, d (see Fig. 1), is an important issue. The trenches violate the order in the periodic structure and cause a redistribution of the local current density during etching. It has been shown that distortion of the photonic crystal lattice around the defect can be minimized by following certain rules.[28,29] Too small a value of d can give a fragile trench, or a trench that reduces with depth; too large a value of d can lead to a wide trench with strongly corrugated walls and a reduced size of pores next to the trench. The optimal value of the parameter d is around a; the width of the trench is of approximately $2r$.

The trenches define rectangular areas of the sample which were removed after detachment of the substrate (see Fig. 1). The resulting PCS is aligned along Γ-K direction of the photonic crystal lattice and consists of 11 pore rows terminated with a silicon prelayer of width $w = d - r$. The photomask defines $d = 4.25\ \mu\mathrm{m}$ ($d/a = 1.13$), which for $r = 0.45a$ gives $w = 0.68a$.

Photoelectrochemical etching was performed in an aqueous solution containing 4% hydrofluoric acid (HF) + 5% ethanol at 20 °C with backside illumination. A constant radius mode was used, with an initial current density $j = 10\ \mathrm{mA/cm^2}$.[30]

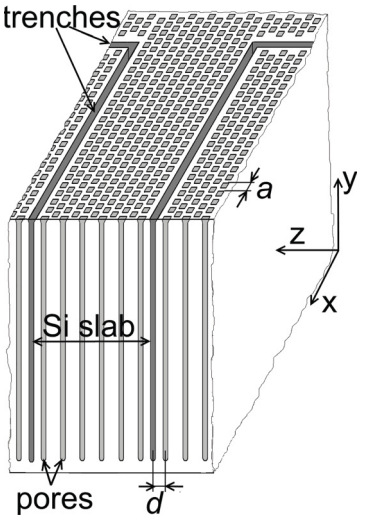

FIG. 1. Schematic of the PCS structure after photoelectrochemical etching of macropores and trenches.

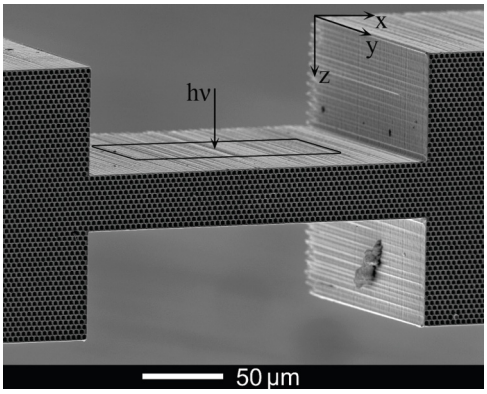

FIG. 2. Scanning electron microscopy image of the two-dimensional photonic crystal slab.

The etching process leads to the formation of air cylindrical pores of radius $r = 1.4\ \mu$m and trenches of width 2.93 μm. The etching depth was about 180 μm. Increase of the etching current density to the critical value of[30,31] $j_{PS} = 31\ \mathrm{mA/cm^2}$ and higher leads to the separation of the porous layer from the substrate and the formation of a free-standing membrane. In order to increase the pore filling factor r/a, the structures were oxidized in a wet-steam atmosphere at a temperature of 1100 °C with subsequent dissolution of the oxide in HF solution. Figure 2 shows the scanning electron microscopy (SEM) image of the resultant structure of the PCS. The samples were then glued to a sample holder allowing measurement of the reflection and transmission spectra.

Fourier transform infrared (FTIR) measurements were performed in the range 650–6500 $\mathrm{cm^{-1}}$ with a resolution of 8 $\mathrm{cm^{-1}}$ using a Digilab FTS 6000 spectrometer in conjunction with a UMA 500 infrared microscope. A gold coated glass slide was used as a 100% reflection reference. A rectangular aperture of $50 \times 200\ \mu\mathrm{m^2}$ for the IR beam was used to provide a reasonable signal to noise ratio. FTIR measurements were made with a polarizer placed in front of the MCT (Mercury, Cadmium, Telluride) detector attached to the microscope. The incident light beam was focused on the sample. The angles of incidence were from 10° to 30° in XZ incidence plane and due to the long rectangular aperture of the beam did not exceed 8° in YZ incidence plane.

III. DETAILS OF CALCULATION

The PCS structure is considered to be infinitely extended in X and Y directions and having a finite number of periods along the Z direction of light incidence, see the explanation of the axes in Fig. 1 and Fig. 2. The scattering matrix (SM) method includes splitting the PCS into elementary planar layers, homogeneous in Z direction. Figure 3 explains this splitting. The circular cross section of each pore is approximated by a staircase. Each elementary layer is homogeneous in Y and Z directions and 1D periodic or homogeneous in X direction, depending whether it belongs to pore or unmodulated material (air or silicon). The solutions to Maxwell's equations for each layer are found by expansion of the electric and magnetic fields into Floquet-Fourier modes (plane waves). The exact solution can be presented as an infinite series over these modes, in

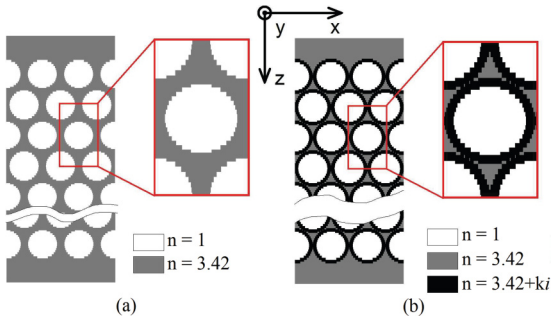

FIG. 3. (Color online) (a) Two-component and (b) three-component models of a 2D PCS with an absorbing ring.

the limit of infinite number of steps per each pore. In order to determine the SM numerically, we have to take a finite number of stairs per pore (as small as 20 stairs appeared to be sufficient) and to truncate the Fourier series on a finite number of plane waves N_g. Then the solutions for each layer must be connected to each other via the boundary conditions. The calculation accuracy increases with an increasing number of plane waves N_g, however, calculation time grows quickly as N_g^3. Nevertheless, for PCSs, fabricated as alternating layers of dielectric and semiconductor components with a relatively small number of layers, the calculations can be performed over a reasonable time scale. We used $N_g = 29$ in what follows.

SM calculations of the reflection spectra without accounting for surface roughness were made first for an idealized *two-component* model structure, shown schematically in Fig. 3(a). The structure, shown in Fig. 3(a), is nonabsorbing, since we are interested in the middle and far-infrared range where the bulk Si is transparent.

In order to simulate the pore roughness, we proposed[32] a *three-component* model for 2D PCSs explained in Fig. 3(b). In the three-component model, an absorbing ring around a pore has been introduced to model light losses due to roughness of the cylindrical air/silicon interface on a scale comparable with λ. It was shown in Ref. 32 that for a 2D photonic crystal lattice with a period of 8 μm, a ring width $\Delta r = 0.8$ μm and a refractive index, $3.42 + 0.2i$, gives a very good fit between the calculated and measured reflection spectra in the region outside the fundamental photonic stop band. In the present study, the period of the fabricated structures is 3.75 μm, allowing us to register the 1st (fundamental) photonic stop band in the wavelength range 7–15 μm. We use the same approach as in Ref. 32 to simulate the influence of roughness on the reflection and transmission spectra.

IV. SIMULATION RESULTS

A 2D PCS with a triangular lattice of 11 rows of air cylinders and with a lattice period a is characterized by two geometrical parameters: the radius of the cylinders, r, and the distance between the centers of the first row of cylinders and a plane separating the PCS from air, w, denoted the interfacial layer thickness. Different surface terminations of the sample for different values of w are shown in Fig. 4. If $w > r$, the PCS is separated from air by a homogeneous layer of silicon, while at $0 \leqslant w < r$ the surface is corrugated. Our goal was to investigate the influence of the geometrical

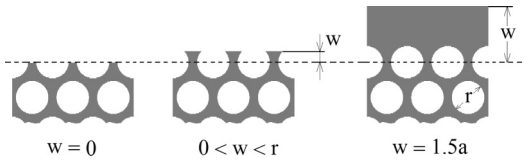

FIG. 4. Surface termination of the PCS for different values of the parameter w.

parameters described on the reflection spectra of 2D PCSs. All calculations were performed for a normal angle of light incidence in the Γ-M direction because the fabricated structure edges were oriented along the Γ-K direction, orthogonal to the Γ-M direction. The results of calculations of the reflection spectra of the investigated structures for $r = 0.45a$ and $w = 0$ are shown in Figs. 5(a) and 5(b) for TM and TE polarizations. We use the notation TM polarization if the electric vector of the incident light is oriented parallel to the macropore channels, and TE polarization if the electric vector is perpendicular to them. It can be seen that the spectra contain regions of high reflection (for $a/\lambda = 0.29$–0.50 in TE polarization and for $a/\lambda = 0.26$–0.30, $a/\lambda = 0.41$–0.52, and $a/\lambda = 0.55$–0.64 in TM polarization) and regions with reflection coefficient oscillations between these high reflection regions. The high-reflection regions arise due to the stop bands of the 2D photonic structure. The oscillations of the reflection coefficient outside the stop bands are the Fabry-Pérot resonances for the light passing through the PCS.

In order to investigate the influence of pore radius on reflection spectra, the reflection spectra of 2D PCS with 11 rows of pores were calculated with parameter $w = 0$ and r varying from $0.1a$ to $0.55a$. The results of these calculations are shown in Figs. 5(c) and 5(d) as reflection maps, see the shades of gray bar for explanation of the scale. It can be seen that the TE reflection spectra have the lowest stop band at $0.1a < r < 0.52a$. The width of the lowest stop band reaches a maximum at $r = 0.45a$. The maximum width of the lowest

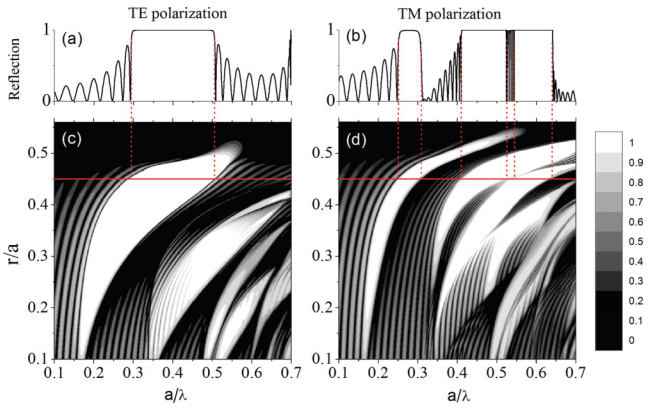

FIG. 5. (Color online) Reflection spectra of a 2D PCS in (a) TE and (b) TM polarization calculated using a two-component model, $r = 0.45a$, $w = 0$, Γ-M direction. Reflection coefficient in TE (c) and TM (d) polarizations of a 2D PCS as a function of the radius of pores, $r = (0.1$–$0.55)a$ and a/λ, for $w = 0$ interfacial layer thickness. The PCS thickness is 11 periods. Red solid and dashed lines show the correspondence between the top and bottom panels. The grey-shades scheme is explained in the bar in the right.

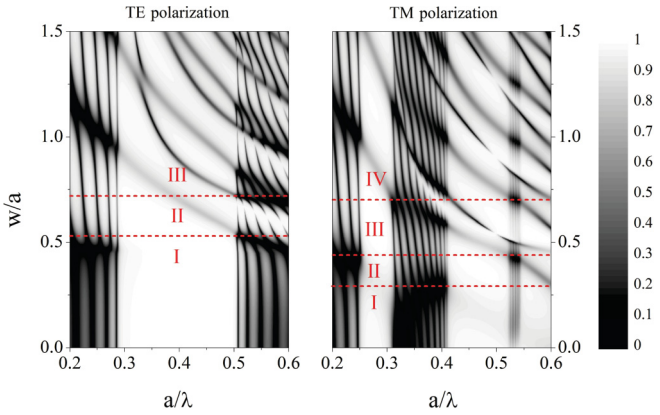

FIG. 6. (Color online) Calculated reflection coefficient in TE and TM polarizations of a 2D PCS as a function of the interfacial layer thickness, w, and a/λ, for $r = 0.45a$, Γ-M direction. Dashed lines and Roman numbers mark the different zones discussed in the text. The grey-shades scheme is explained in the bar in the right.

stop band using TM polarization is reached at $r = 0.43a$, whereas the widest second stop band is provided by a pore radius $r = 0.47a$.

Let us investigate the influence of the interface on the reflection spectra. For this, we fixed the radius of the cylinders at $0.45a$ and varied the parameter w in the range 0–$1.5a$. The results of these calculations with a two-component model are shown in Fig. 6. From Fig. 6 it can be seen that the calculated reflection spectra in the range $a/\lambda =$ 0.2–0.6 consist of stop bands, Fabry-Pérot oscillations and, additionally, dips within the high reflection regions. The widths and the positions of the stop bands do not depend on the thickness of the air/PCS interface. Hence, for fixed a, the pore radius is the only parameter which is responsible for the widths and positions of the photonic stop bands. The period of the Fabry-Pérot oscillations decreases slightly with an increase of interfacial layer thickness. This is expected since the period of the Fabry-Pérot oscillations is inversely proportional to the total sample thickness. The most interesting behavior is demonstrated by the reflection dips inside the photonic stop bands. The dip position depends on w, the air/PCS interface thickness. The TE reflection (TM reflection) map can be divided into three (four) zones by the number of these dips in the spectrum, as shown in Fig. 6. The TE stop band in the zone I-TE does not have these dips. The first dip appears at $w = 0.55a$. The position of the first dip shifts towards lower wave numbers with increasing w and reaches the left edge of the stop band at $w = 0.92a$. The high-reflection region has only one dip for $0.55a < w < 0.72a$ (zone II-TE). For $w > 0.72$ (zone III-TE), the high-reflection region has two or more dips. Similar behavior is observed using TM polarization. The results shown in Fig. 6 are very important for the fabrication of structures with triangular lattice of air pores in silicon. Indeed, from Fig. 4, the surface termination of a 2D PCS is flat when $w > r$. In this case, $w > 0.45a$. At the same time, a "pure" stop band in the TE reflection spectra, i.e., a stop band without surface dips, exists only for $w < 0.55a$ (zone I-TE). Thus the range of the values of parameter w which provides the flat surface termination and a "pure" photonic stop band is $0.45a < w < 0.55a$.

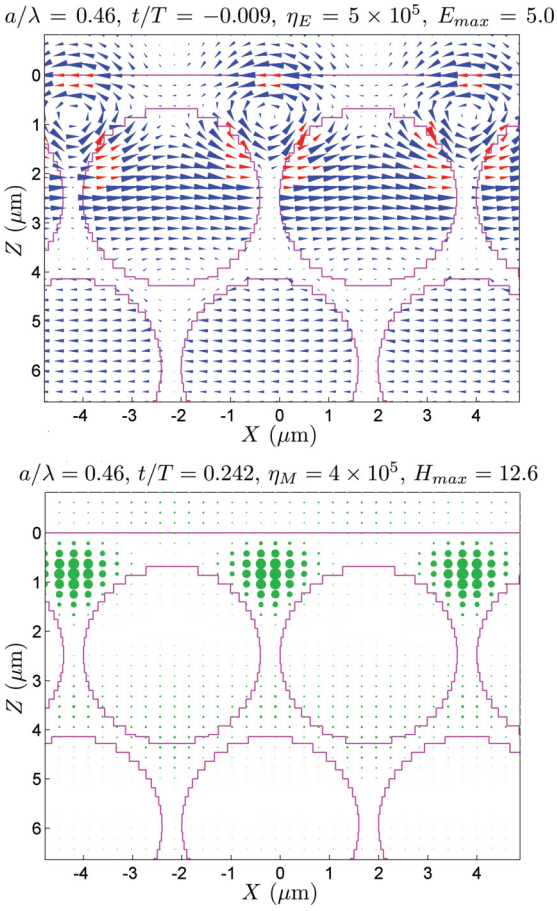

FIG. 7. (Color online) Calculated spatial distributions of the electric [blue and red cones in (a)] and magnetic [green circles in (b)] fields in 2D PCS for normal incidence of TE polarized light. The length of the cones (circles area) is proportional to the field strength at the central point of each cone (circle). Cones specify the corresponding electric field direction by their orientation. The magnetic field in the TE polarization is along Y. Fields are shown for an incoming frequency $a/\lambda = 0.466$ corresponding to the dip in the photonic stop band for TE polarization. $r = 0.45a$, $w = 0.62a$. The calculation was performed for $a = 4$ μm.

In order to understand the origin of the dips in the reflection spectra, we calculated the electromagnetic near-field distribution in the 2D PCS. We will limit our discussion to structures of period $a = 4$ μm with a pore radius $r = 0.45a$, an interfacial layer thickness $w = 0.62a$, TE polarization and a normal light incidence. The spatial electric and magnetic field distributions in the near-surface region are shown in Fig. 7 for $a/\lambda = 0.46a$, which corresponds to the position of the dip inside the photonic stop band in the TE reflection spectra. The method used to present the electromagnetic field is described in Ref. 33. The electric and magnetic field vectors are shown in Fig. 7 as a two-dimensional array of cones and circles (actually a face on views of cones perpendicular to the image plane).

The size of the cones is proportional to the field strength at the center of each cone. The length of the blue cones is scaled to the amplitude of the incoming wave in vacuum; in a case of red cones, it is reduced by two, to prevent cone overlap. Note that the electric and magnetic fields are depicted at the instant t (measured in units of light period T and shown in the

title of each panel) when the field intensities, integrated over the displayed cross sections, reach a maximum. $E_{\max}$ ($H_{\max}$) is the maximum field measured in units of the incoming wave amplitude (i.e., it shows the field enhancement in the near-field zone). It can be seen that the electric and magnetic fields are localized in the near-surface region. Note that electric field in this region takes the shape of vortices located between the upper pores. The maxima of the magnetic fields are in the centers of these vortices. The time difference between the part at which electric and magnetic fields becomes maximal is approximately a quarter of the oscillation period, $t \approx 0.25T$. Hence, the field distribution, shown in Fig. 7, corresponds, in the main, to a standing wave. The ratio between the maximal and minimal electric (magnetic) field energies over the period of electromagnetic oscillation η_E (η_M), a so-called field modulation coefficient, are also shown in the title of Fig. 7. The η_E and η_M values exceed unities by several orders of magnitude. This is also characteristic of the standing wave of the surface mode. The mode described here is a surface Tamm state:[34] it arises in the stop band due to the total light reflection from the silicon/photonic crystal interface and exponentially decreases inside it. However, it is open for radiative losses on the other partially reflecting air/Si interface and thus differs from the usual Tamm electronic states on the solid/vacuum interface. Such modes have been considered, e.g., in Ref. 7 and are characterized by a small quality factor (as Fabry-Pérot modes).

V. EXPERIMENTAL RESULTS

Experimental reflection spectra for TE and TM polarizations are shown in Figs. 8(a) and 8(b). Theoretical spectra, calculated for a fixed angle of light incidence of 20° with two- and three-component model, are shown by the dotted and solid lines in Figs. 8(c) and 8(d). The widths and positions of the photonic stop bands in the theoretical reflection spectra coincide with those in the experimental spectra. The theoretical spectra demonstrate one dip in the first stop band of the TE spectrum ($a/\lambda = 0.477$) and one dip in the second stop band of the TM spectrum ($a/\lambda = 0.491$). The amplitude of the dip in the TE reflection spectrum for two-component model is 0.07, rendering it invisible on this scale. From an analysis of the theoretical results shown in Fig. 6, these dips are associated with the surface modes.

The spectral positions of surface dips in the experimental and theoretical spectra coincide with each other. However, there is some disagreement between experimental and theoretical spectra calculated by the two-component model, in particular in the amplitudes of the surface dips. As already mentioned, the reason for this disagreement may be Rayleigh scattering of light on the rough inner surfaces of the air pores. In order to simulate the scattering losses, we used a three-component model [see Fig. 3(b)]. Another reason for the mismatch between the theoretical and experimental spectra is the deviation of the angle of incidence of light from normal. In order to take these factors into account, we calculated the reflection spectra using a three-component model for various angles of incidence in accordance with the shape of the incident light beam. Because the incident light spot has a long rectangular shape, with an aspect ratio of 4:1, we consider only those directions of incident light that are perpendicular to the

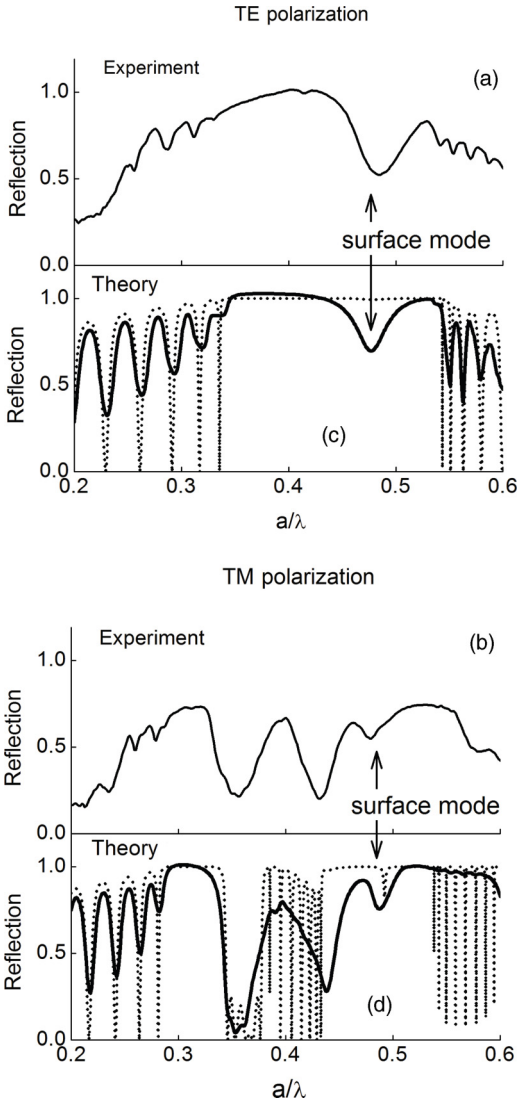

FIG. 8. (a, b) Experimental and (c, d) theoretical reflection spectra of a 2D PCS for TE and TM polarizations. Parameters of calculation: $r = 0.47a$ and $w = 0.62a$. In (c) and (d) the dotted (solid) lines denote the reflection spectra calculated using a two-component (three-component) model. $\Delta r = 0.4\ \mu$m, $n_{\text{abs}} = 3.42 + 0.03i$.

axes of the air cylinders. The calculated spectra were integrated over angles of incidence from 10° to 30° in XZ incidence plane with the weight coefficients specified in Ref. 35. The result of this integration is shown in Figs. 8(c) and 8(d) by a solid line. From Figs. 8(c) and 8(d), the theoretical reflection spectra obtained are in very good agreement with the experimental spectra.

The experimental and theoretical transmission spectra of the investigated structure are presented in Fig. 9. The transmission spectra have regions of low-transmission, which are associated with photonic stop bands. Since the intensity of the electromagnetic field decreases with depth of the photonic crystal slab (see Fig. 7), the surface-related peaks in the transmission spectra are very weak and cannot be recognized experimentally. The discussed above reflection dips are due to roughness losses which have peaks at the corresponding wavelengths.

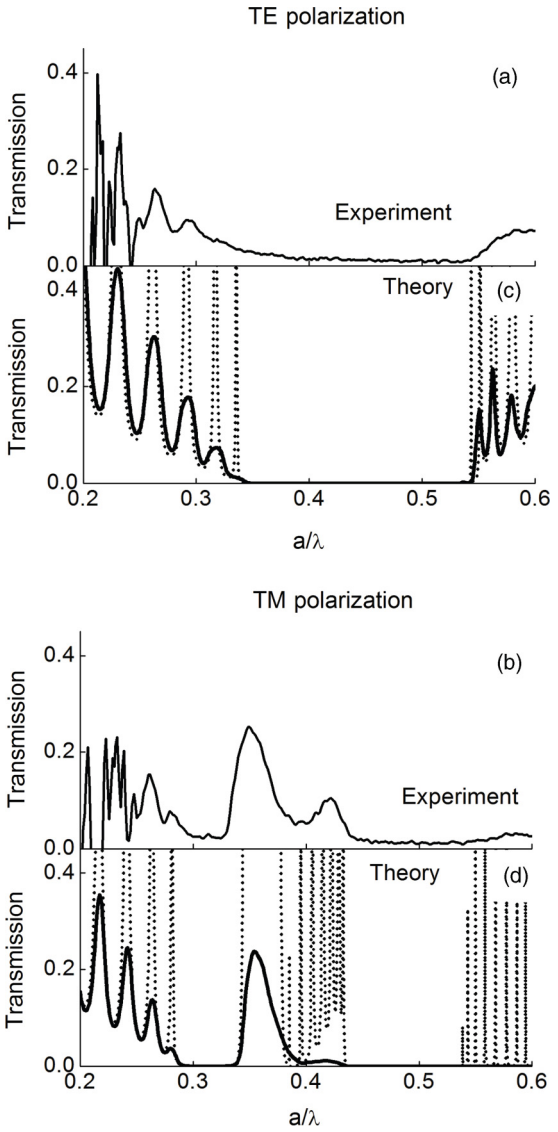

FIG. 9. (a, b) Experimental and (c, d) theoretical transmission spectra of 2D PCS for TE and TM polarizations. Parameters of calculation: $r = 0.47a$ and $w = 0.62a$. In (c) and (d) the dotted (solid) lines denote the transmission spectra calculated using a two-component (three-component) model. $\Delta r = 0.4$ μm, $n_{\text{abs}} = 3.42 + 0.03i$.

Note that the calculation of the reflection and transmission spectra by the three-component model implies the use of the following fitting parameters: the width of the absorbing ring around pores, Δr, and the refractive index of the absorbing ring material material, n_{abs}. The best agreement between experimental and theoretical spectra is achieved using $\Delta r = 0.4$ μm and $n = 3.42 + 0.03i$. Use of these values as fitting parameters enabled us to calculate loss sensitive features of the reflection spectra such as the amplitudes of the surface dip.

VI. DISCUSSION

It was shown that the accounting for the roughness allows to calculate the amplitude of the surface reflection dips correctly. This fact can be understood in terms of a model of asymmetric Fabry-Pérot resonator. Let us consider a homogeneous silicon

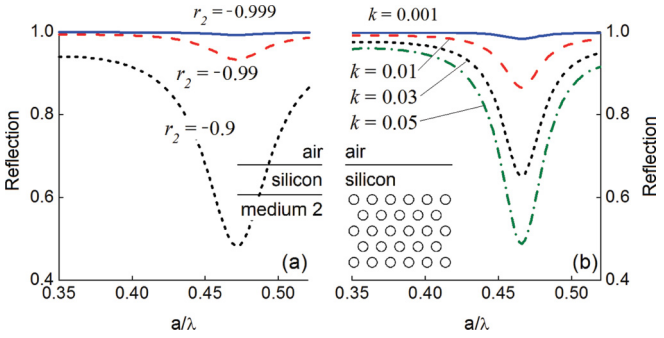

FIG. 10. (Color online) Reflection spectra (a) of the asymmetric resonator structure for different reflection coefficients, r_2, between medium 2 and silicon and (b) of the photonic crystals structure for different extinction coefficients k of the absorbing ring. Parameters of the asymmetric resonator: the thickness of silicon layer is $0.62a$ and the normal angle of light incidence. Parameters of the PCS: $r = 0.47a$, $w = 0.62a$, $\Delta R = 0.4$ μm, 11 pore rows, angle of light incidence is 20°, TE polarization.

layer with a refractive index $n = 3.42$ and of thickness h, terminated by two homogeneous media, namely, air and medium 2 [see inset in Fig. 10(a)]. The layer of silicon in this model can be considered as an interfacial layer separating medium 2 from the air. For a normal incidence of light, the reflection coefficient of the model structure is determined by the following expression:

$$R \equiv |r_0|^2 = \left| \frac{r_1 e^{-i\beta} + r_2 e^{i\beta}}{e^{-i\beta} + r_1 r_2 e^{i\beta}} \right|^2, \qquad (1)$$

where r_1 is the Fresnel reflection coefficient at the interface between air and silicon layer, r_2 is the reflection coefficient at the interface between the silicon layer and medium 2 and $\beta = 2\pi nh/\lambda$. From the Fresnel equations, it follows that the parameter $r_1 = -0.55$. Let us take $|r_2|$ close to 1 [which can be modeled by a large refractive index of the medium 2: $n_2 = (1 + |r_2|)(1 - |r_2|)n_{\text{Si}}$] and also take into account the π phase shift of the light reflected from the silicon/medium 2 interface. The reflection coefficient as a function of a/λ[36] is shown in Fig. 10(a) for three values of the parameter r_2, namely, -0.999, -0.99, and -0.9, where minus accounts for the π phase shift of reflection discussed above. In fact, the curves from Fig. 10(a) are simply the Fabry-Pérot resonances in this asymmetric structure. The presence of the silicon interfacial layer gives rise to dips in the reflection spectrum and the amplitude of these dips increases as values of parameter $|r_2|$ decrease from unity.

This situation is similar to that occurring for the 2D PCSs investigated, where medium 2 is photonic crystal. Figure 10(b) demonstrates that the amplitude of the surface dip in the reflection spectra of the PCS decreases with increase of the extinction coefficient of the absorbing ring in the three-component model. It means that the amplification of the surface dip in the reflection spectra of a PCS is caused by non-100% reflection from the photonic crystal area in the spectral range of the stop band. In principle, the deviation of the parameter r_2 from unity for photonic crystals is due to two factors. Firstly, the number of pore rows is not infinite. The presence of surface dips in the reflection spectra of the

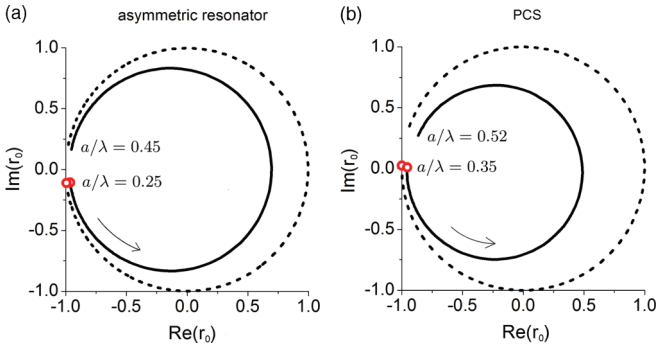

FIG. 11. (Color online) Dependence of imaginary part of the complex amplitude reflectance, $\mathrm{Im}(r_0)$, vs the real part of the complex amplitude reflectance, $\mathrm{Re}(r_0)$, for (a) an asymmetric resonator and (b) a 2D PCS. Parameters of the structures and the incident light correspond to those in Fig. 10. Calculations were performed using a two-component model (dashed line) and a three-component model for $k = 0.1$ (solid line). The red circles denote the initial values of a/λ.

two-dimensional photonic crystal structure without roughness (two-component model) is due to the finite thickness of the 2D PCS. The second factor is the presence of roughness on the inner surface of the pores and other geometrical imperfections. From Fig. 8(c), the amplitude of the surface dip due to the finite thickness of the 2D PCS is of the order of 10^{-2}. At the same time, the experimental value of the amplitude of the surface dip is 0.25. Hence, the second factor, is predominant. In the absence of roughness related scattering losses, some of the surface dips in the reflection spectra have a very small amplitude and are invisible on the scale of the spectra shown here. In this case, identification of the Tamm states requires measurement of the phase shift of the reflected signal.

The calculated dependence $\mathrm{Im}[r_0(a/\lambda)]$ versus $\mathrm{Re}[r_0(a/\lambda)]$, where r_0 is the complex amplitude reflectance, is shown in Fig. 11(a) for the layered asymmetric resonator and for the 2D PCS with $r = 0.45a$, $w = 0.62a$. In these calculations, the range of variation of a/λ is 0.25–0.45 for asymmetric resonator and 0.35–0.52 for 2D PCS. The latter corresponds to the high-reflection region of the 2D PCS (see Fig. 8). From Fig. 6, these values of r and w correspond to the presence of one surface dip in the TE stop band of the reflection spectrum. In both cases, the asymmetric resonator and the 2D PCS, the relative phase of the reflected signal changes by a value of almost 2π with an increase of a/λ from initial value to the final one. It can be seen that non-100% reflection at the interface between silicon layer and medium 2 and between nonstructured silicon layer and photonic crystal area affects the absolute value of r_0 and hardly changes the phase shift of the complex amplitude reflectance. Thus the presence of surface states in 2D PCS can be confirmed by measuring the relative phase of the reflected signal.

VII. CONCLUSIONS

Reflection and transmission spectra of two dimensional photonic crystal slabs with various surface terminations have been investigated theoretically and experimentally. The presence of the homogeneous silicon interfacial layer, separating the 2D PCS from air, gives rise to the dips within the photonic stop bands of the reflection spectra in TE and TM polarizations. The spatial distribution of the electromagnetic field in the structures investigated shows that these dips correspond to the photonic surface Tamm states. It was shown that the roughness of the inner surfaces of pores affects the amplitude of the surface-associated dips in the reflection spectra. Absolutely smooth inner surfaces of pores would make the observation of the surface modes within the stop band of the reflection spectrum impossible. Furthermore, it was demonstrated that the phase of the reflected light changes by 2π when the frequency of the incident light passes the frequency of the corresponding surface mode. Thus, this mode can be observed by measurements of the phase shift upon reflection even from an ideal system without losses. A simulation of the roughness of the cylindrical surfaces of the air/silicon interface as well as the deviation of the angle of light incidence from normal enabled us to achieve a satisfactory agreement between the experimental and theoretical spectra of 2D PCSs.

ACKNOWLEDGMENTS

This work was supported by Russian Foundation for Basic Research and the Russian Academy of Sciences. S.D. acknowledges Irish Research Council for Science, Engineering and Technology (IRCSET) and Trinity College Dublin for financial support. A.B. acknowledges the financial support from IRCSET's International Centre for Graduate Education in Micro and Nano-Engineering (ICGEE). G.L. thanks Presidential grant for Russian Scientific schools, NSh-3008.2012.2.

*Corresponding author: perovat@tcd.ie

[1] N. Malkova and C. Z. Ning, Phys. Rev. B **73**, 113113 (2006).
[2] A. P. Vinogradov, A. V. Dorofeenko, S. G. Erokhin, M. Inoue, A. A. Lisyansky, A. M. Merzlikin, and A. B. Granovsky, Phys. Rev. B **74**, 045128 (2006).
[3] N. Malkova and C. Z. Ning, J. Phys.: Condens. Matter **19**, 056004 (2007).
[4] E. Moreno, F. J. García-Vidal, and L. Martin-Moreno, Phys. Rev. B **69**, 121402 (2004).
[5] A. Namdar, I. V. Shadrivov, and Y. S. Kivshar, Appl. Phys. Lett. **89**, 114104 (2006).
[6] Y. S. Kivshar, Laser Phys. Lett. **5**, 703 (2008).
[7] A. P. Vinogradov, A. V. Dorofeenko, A. M. Merzlikin, and A. A. Lisyansky, Phys. Usp. **53**, 243 (2010).
[8] P. Yeh, A. Yariv, and A. Cho, Appl. Phys. Lett. **32**, 104 (1978).
[9] F. Lederer, L. Leine, R. Muschall, T. Peschel, C. Schmidt-Hattenberger, T. Trutschel, A. Boardman, and C. Wachter, Opt. Commun. **99**, 95 (1993).
[10] N. Malkova, I. Hromada, X. Wang, G. Bryant, and Z. Chen, Opt. Lett. **34**, 1633 (2009).
[11] T. Decoopman, G. Tayeb, S. Enoch, D. Maystre, and B. Gralak, Phys. Rev. Lett. **97**, 073905 (2006).

[12]S. Xiao, M. Qiu, Z. Ruan, and S. He, Appl. Phys. Lett. **85**, 4269 (2004).
[13]A. Mihi, H. Míguez, I. Rodríguez, S. Rubio, and F. Meseguer, Phys. Rev. B **71**, 125131 (2005).
[14]D. Pergande, T. M. Geppert, A. von Rhein, S. L. Schweizer, R. B. Wehrspohn, S. Moretton, and A. Lambrecht, J. Appl. Phys. **109**, 083117 (2011).
[15]D. Pergande, A. von Rhein, T. Geppert, and R. Wehrspohn, J. Comput. Theor. Nanos. **6**, 1993 (2009).
[16]R. M. A. Azzam and N. M. Bashara, *Ellipsometry and Polarized Light*, Vol. 31 (North Holland, 1987).
[17]R. M. A. Azzam and N. M. Bashara, Phys. Rev. B **5**, 4721 (1972).
[18]A. A. Maradudin and D. L. Mills, Phys. Rev. B **11**, 1392 (1975).
[19]H. Benisty, D. Labilloy, C. Weisbuch, C. J. M. Smith, T. F. Krauss, D. Cassagne, A. Beraud, and C. Jouanin, Appl. Phys. Lett. **76**, 532 (2000).
[20]H. Benisty, P. H. Lalanne, S. Olivier, M. Rattier, C. Weisbuch, C. J. M. Smith, T. F. Krauss, C. Jouanin, and D. Cassagne, Opt. Quant. Electron. **34**, 205 (2002).
[21]S. A. Dyakov, E. V. Astrova, T. S. Perova, S. G. Tikhodeev, N. A. Gippius, and V. Y. Timoshenko, JETP **113**, 80 (2011).
[22]D. M. Whittaker and I. S. Culshaw, Phys. Rev. B **60**, 2610 (1999).
[23]S. G. Tikhodeev, A. L. Yablonskii, E. A. Muljarov, N. A. Gippius, and T. Ishihara, Phys. Rev. B **66**, 045102 (2002).
[24]N. A. Gippius, S. Tikhodeev, and T. Ishihara, Phys. Rev. B **72**, 045138 (2005).
[25]A. Christ, S. G. Tikhodeev, N. A. Gippius, J. Kuhl, and H. Giessen, Phys. Rev. Lett. **91**, 183901 (2003).
[26]T. Geppert, S. L. Schweizer, U. Gösele, and R. B. Wehrspohn, Appl. Phys. A **84**, 237 (2006).
[27]R. B. Wehrspohn, S. L. Schweizer, and V. Sandoghdar, Phys. Stat. Sol. A **204**, 3708 (2007).
[28]E. V. Astrova, G. V. Fedulova, and E. V. Guschina, Semiconductors **44**, 1617 (2010).
[29]E. V. Astrova, G. V. Fedulova, Y. A. Zharova, and E. V. Gushchina, Phys. Stat. Sol. C **8**, 1936 (2011).
[30]V. Lehmann, *Electrochemistry of Silicon* (Wiley-VCH, D-69469 Weinheim, 2002).
[31]V. Lehmann and H. Föll, J. Electrochem. Soc. **137**, 653 (1990).
[32]S. A. Dyakov, E. V. Astrova, T. S. Perova, V. A. Tolmachev, G. V. Fedulova, A. Baldycheva, V. Y. Timoshenko, S. G. Tikhodeev, and N. A. Gippius, in Proc. SPIE **7943**, 79431I (2011).
[33]A. Christ, T. Zentgraf, J. Kuhl, S. G. Tikhodeev, N. A. Gippius, and H. Giessen, Phys. Rev. B **70**, 125113 (2004).
[34]I. E. Tamm, Phys. Z. Sowietunion **1**, 733 (1932).
[35]S. A. Dyakov, V. A. Tolmachev, E. V. Astrova, S. G. Tikhodeev, V. Y. Timoshenko, and T. S. Perova, in Proc. SPIE **7521**, 75210G (2009).
[36]In fact, the asymmetric resonator structure is not characterized by the parameter a, which denotes the period of the photonic crystal structure. However, the reflection spectra are plotted with respect to a/λ to ensure a better correspondence between Figs. 10(a) and 10(b).